REPORT DOCUMENTATION PAGE

Form Approved

OMB No. 0704-0188

1. REPORT DATE *(DD-MM-YYYY)*	2. REPORT TYPE	3. DATES COVERED *(From - To)*
02-01-2015	Final	26 Aug 2013 to 25 Aug 2014

4. TITLE AND SUBTITLE

Nucleation and growth control of ZnO via impurity-mediated crystallization

5a. CONTRACT NUMBER
FA2386-13-1-4111

5b. GRANT NUMBER

5c. PROGRAM ELEMENT NUMBER

6. AUTHOR(S)

Dr. Naho Itagaki

5d. PROJECT NUMBER

5e. TASK NUMBER

5f. WORK UNIT NUMBER

7. PERFORMING ORGANIZATION NAME(S) AND ADDRESS(ES)
Kyushu University
744 Motooka, Nishi-ku,
Fukuoka 819-0395
Japan

8. PERFORMING ORGANIZATION REPORT NUMBER
N/A

9. SPONSORING/MONITORING AGENCY NAME(S) AND ADDRESS(ES)

AOARD
UNIT 45002
APO AP 96338-5002

10. SPONSOR/MONITOR'S ACRONYM(S)
AFRL/AFOSR/IOA(AOARD)

11. SPONSOR/MONITOR'S REPORT NUMBER(S)
AOARD-134111

12. DISTRIBUTION/AVAILABILITY STATEMENT

Distribution Code A: Approved for public release, distribution is unlimited.

13. SUPPLEMENTARY NOTES

14. ABSTRACT
The primary objective is to develop a fabrication method of ZnO based on magnetron sputtering, “impurity-mediated crystallization (IMC)”, where crystal nucleation and the growth are controlled by adsorbed impurities on the growth surface. By utilizing ZnO films prepared by IMC method as buffer layers (IMC buffer layers), two kinds of high-quality ZnO based semiconductors have been fabricated, the properties of which are superior to those of conventional ZnO films fabricated without IMC buffer layers.

15. SUBJECT TERMS

impurity-mediated crystallization , c-sapphire substrates , metalorganic, morphology, Rutherford backscattering spectrometry, X-ray photoelectron spectroscopy , Hall-effect measurement

16. SECURITY CLASSIFICATION OF:			17. LIMITATION OF ABSTRACT	18. NUMBER OF PAGES	19a. NAME OF RESPONSIBLE PERSON
a. REPORT	b. ABSTRACT	c. THIS PAGE			Seng Hong, Ph.D.
U	U	U	SAR	15	19b. TELEPHONE NUMBER *(Include area code)* +81-42-511-2000

Standard Form 298 (Rev. 8/98)
Prescribed by ANSI Std. Z39.18

Report Documentation Page

Form Approved
OMB No. 0704-0188

1. REPORT DATE	2. REPORT TYPE	3. DATES COVERED
16 JAN 2015	**Final**	**26-08-2013 to 25-08-2014**

4. TITLE AND SUBTITLE	5a. CONTRACT NUMBER
Nucleation and growth control of ZnO via impurity-mediated	**FA2386-13-1-4111**
	5b. GRANT NUMBER
	5c. PROGRAM ELEMENT NUMBER
6. AUTHOR(S) **Naho Itagaki**	5d. PROJECT NUMBER
	5e. TASK NUMBER
	5f. WORK UNIT NUMBER
7. PERFORMING ORGANIZATION NAME(S) AND ADDRESS(ES) **Kyushu University,744 Motooka, Nishi-ku,,Fukuoka 819-0395,Japan,NA,NA**	8. PERFORMING ORGANIZATION REPORT NUMBER **N/A**
9. SPONSORING/MONITORING AGENCY NAME(S) AND ADDRESS(ES) **AOARD, UNIT 45002, APO, AP, 96338-5002**	10. SPONSOR/MONITOR'S ACRONYM(S) **AFRL/AFOSR/IOA(AOARD)**
	11. SPONSOR/MONITOR'S REPORT NUMBER(S) **AOARD-134111**

12. DISTRIBUTION/AVAILABILITY STATEMENT
Approved for public release; distribution unlimited

13. SUPPLEMENTARY NOTES

14. ABSTRACT
The primary objective is to develop a fabrication method of ZnO based on magnetron sputtering, ?impurity-mediated crystallization (IMC)?, where crystal nucleation and the growth are controlled by adsorbed impurities on the growth surface. By utilizing ZnO films prepared by IMC method as buffer layers (IMC buffer layers), two kinds of highquality ZnO based semiconductors have been fabricated, the properties of which are superior to those of conventional ZnO films fabricated without IMC buffer layers.

15. SUBJECT TERMS
impurity-mediated crystallization , c-sapphire substrates , metalorganic, morphology, Rutherford backscattering spectrometry, X-ray photoelectron spectroscopy , Hall-effect measurement

16. SECURITY CLASSIFICATION OF:			17. LIMITATION OF ABSTRACT	18. NUMBER OF PAGES	19a. NAME OF RESPONSIBLE PERSON
a. REPORT **unclassified**	b. ABSTRACT **unclassified**	c. THIS PAGE **unclassified**	**Same as Report (SAR)**	**15**	

FINAL TECHNICAL REPORT

Project No: AOARD 134111
Title: Nucleation and growth control of ZnO via impurity-mediated crystallization
Principal investigator: Naho Itagaki
Affiliation: Graduate School of Information Science and Electrical Engineering, Kyushu University
Address: 744 Motooka, Nishi-ku, Fukuoka 819-0395, Japan

ABSTRACT

We have developed a fabrication method of ZnO based on magnetron sputtering, "impurity-mediated crystallization (IMC)", where crystal nucleation and the growth are controlled by adsorbed impurities on the growth surface. By utilizing ZnO films prepared by IMC method as buffer layers (IMC buffer layers), two kinds of high-quality ZnO based semiconductors have been fabricated, the properties of which are superior to those of conventional ZnO films fabricated without IMC buffer layers. One is single crystalline ZnO films with atomically-flat surfaces that are heteroepitaxially grown on lattice mismatched (18%) sapphire substrates, and the other is poly-crystalline ZnO:Al transparent electrodes with low resistivity (3×10^{-4} Ω·cm @ 20 nm) that are non-epitaxially grown on glass substrates. The crystal growth mechanism of ZnO prepared by IMC method has been also studied by observation of the surface-morphology evolution. In the case of heteroepitaxial growth of ZnO on sapphire substrates, nitrogen atoms introduced as impurities lead to a dense and homogeneous nucleation that efficiently release the strain energy coming from the large lattice mismatch, and resultant IMC buffer layers have smooth surface and good in-plane alignment. On such buffer layers, ZnO crystals, which originate from the grains of the buffer layers, are grown laterally and gradually coalesced, and finally a single crystalline ZnO is formed. From these results, we conclude that IMC method is a powerful tool for growth of high-quality ZnO that can replace rare-metal-based materials in optoelectronic devices such as In_2O_3:Sn as transparent conducting oxides (TCOs) and GaN in light emitting devices, bringing a significant reduction in the cost as well as the reduction of damage to human health and the environment.

1. INTRODUCTION

Oxide semiconductors have attracted much attention because of their advantages such as high transparency and wide-ranging conductivity. ZnO is one of the most fascinating oxide with a wide application range. The low electrical resistivity, the high transparency to visible lights, and the material abundance make ZnO:Al (AZO) a great potential alternative to In_2O_3:Sn (ITO) as transparent conductive oxide (TCO) in flat-panel displays, touch screens on smartphones, organic light-emitting diodes (OLEDs), solar cells, etc [1-6]. The resistivity of AZO fabricated on glass substrates, however, is higher than that of ITO, especially when the film thickness is less than 100nm [1,7]. Since the crystallinity of ZnO films strongly affects both the carrier density and the mobility, fabrication methods of ZnO films with good crystal alignment, large crystal grain size, and low defect density is required.

ZnO has been also recognized as a candidate for high performance ultraviolet light-emitting diodes (LED) and laser diodes (LD) that take advantage of its high exciton binding energy of 60 meV, which is larger than that of the commercial LED material, GaN (25 meV) [8-10]. This large exciton binding energy enables high-efficiency light emission through exciton recombination even at room temperature or higher. Furthermore, due to the material abundance and low toxicity of ZnO, replacement of GaN will bring

significant reduction in the cost as well as the reduction of damage to human health and the environment. Since such devices require single crystals with low defect density, ZnO based LEDs have been fabricated on lattice-matched but expensive substrates such as bulk ZnO and $ScAlMgO_4$ substrates[8,9]. Furthermore, these ZnO films have been fabricated by molecular beam epitaxy (MBE) method that needs ultrahigh vacuum of 10^{-7} Pa. Even though the material cost of ZnO itself is much lower than that of GaN, it is essential to fabricate single crystalline ZnO films on cost-effective substrates by a mass-productive method for replacement of GaN. C-plane sapphire has a great potential as an epitaxial substrate for ZnO because of its low cost and the availability in large area wafers. Due to the large lattice mismatch of 18%, however, ZnO films prepared on sapphire substrates have large crystal mosaics, high residual carrier concentrations, and low mobility, all of which make optoelectronic applications challenging [11].

This research aims to establish methods of fabricating i) single-crystalline ZnO films on c-plane sapphire substrates and ii) poly-crystalline low-resistive ZnO based TCOs on glass substrates, which are highly competitive with rare-metal-based materials such as GaN and In_2O_3:Sn, by a cost-effective deposition technique. For this purpose, magnetron sputtering with working pressure of 0.1-1 Pa, which has great advantages in terms of mass production, was employed for film deposition.

One of the most promising means to improve the crystal quality of ZnO films is to prepare buffer layers prior to the crystal growth. Various types of ZnO buffer layers have been reported. Khranovsky et al. fabricated highly oriented ZnO (002) films on c-sapphire substrates by incorporating low temperature (LT) ZnO buffer layers prepared by metalorganic chemical vapor deposition [12]. In that work, X-ray diffraction (XRD) 2θ-ω patterns showed only the (002) diffraction peak, whereas ZnO films without the buffer layers showed the (100) and (101) diffraction peaks aside from (002) peak. Similarly, Nakamura et al. fabricated ZnO films by pulsed-laser deposition on LT buffer layers on c-plane substrates.[13] With buffer layers deposited at 500°C, the full-width half-maximum (FWHM) of the (002) rocking curve decreased to 0.09° from 0.2–0.3°, indicating that well aligned ZnO films were fabricated. These results certainly demonstrate that buffer layers improve the crystal quality of ZnO films. Single crystalline ZnO films with desired properties for homojuncion LED/LD have, however, not been obtained yet. The idea of LT buffer layers was first reported by Amano et al., having been practically used for fabrication of GaN based LED on sapphire substrates, where the lattice mismatch between GaN and sapphire is large of 16% [14]. The role of the LT buffer layers is to provide high density of nucleation site and smooth surface, and thus to reduce the interfacial free energy between GaN and the substrates that comes from the large lattice mismatch. The nucleation control of the LT buffer layers is carried out through deposition of amorphous films at a temperature sufficiently lower than the crystal growth temperature and annealing them. Such buffer layers enhance the lateral growth of subsequently grown GaN, as a result, single crystalline GaN films are fabricated. In the case of ZnO, however, LT buffer layers have limited effects on the improvement of the crystal quality because the amorphous phase of ZnO is difficult to obtain even at room temperature because of the low crystallization temperature. This is apparent when a sputtering method is employed for film deposition, where the high energy of impingement of sputtered species as well as negative oxygen ions and recoil argons exists.

In this research, a new buffer layer fabricated via impurity-mediated crystallization (IMC) is proposed, where the nucleation and the growth of ZnO crystals are controlled by controlling adsorption/desorption behaviour of impurity atoms on the growth surface, instead of lowering the deposition temperature.

2. EXPERIMENTAL

2.1 Heteroepitaxial growth of single crystalline ZnO films on c-plane sapphire substrates

2.1.1 Fabrication of IMC buffer layers on c-plane sapphire substrates

IMC buffer layers were deposited on 10×10 mm^2 c-plane sapphire substrates by RF magnetron sputtering. The target-substrate distance was 74.5 mm. ZnO ceramic targets (2 inch in diameter) were used, and the RF power supplied to each target was 100 W. The substrate temperature was 680-780°C. Ar-N_2 mixed gas with N_2/(Ar+N_2) flow rate ratio of 0.08 was used and the total gas pressure was 0.30 Pa. For comparison, ZnO buffer layers were fabricated in Ar/O_2 atmosphere ("conventional buffer layers") with the same sputtering system. The thickness of buffer layers was 10 nm, confirmed by X-Ray Reflectometry (XRR, Bruker D8 Discover). The nitrogen concentration in the films fabricated in this study was below the detection limit of X-ray fluorescence (XRF) spectrometer (Rigaku ZSX Primus II), attributed to the high substrate temperature that activates desorption of nitrogen species from the growth surface of ZnO films [15]. The surface morphologies were investigated by tapping mode atomic force microscopy (AFM, Veeco Nanoscope II).

2.1.2 Fabrication of single crystalline ZnO films on IMC buffer layers

Single crystalline ZnO films were grown on buffer layers with the same sputtering system as that used for buffer layer deposition. ZnO ceramic targets (2 inches in diameter) were used and the RF power supplied to each target was 60 W. The substrate temperature was kept at 700°C. Ar-O_2 mixed gas with an O_2/(Ar+O_2) flow rate ratio of 0.10 was used, and the total deposition pressure was 0.70 Pa. For comparison, ZnO films that were deposited directly on sapphire substrates without buffer layers were prepared under the same deposition conditions. From scanning electron microscopy (SEM) observation, it was confirmed that the film thickness of ZnO films was 1 μm. The crystallinity of all the films was evaluated by X-ray diffraction (XRD) using a four-circle texture diffractometer (Bruker D8 Discover), and a Cu Kα source (λ = 0.154 nm). The surface morphologies were investigated by tapping mode AFM. Electrical properties were evaluated by Hall-effect measurement by using the four-point van der Pauw configuration at room temperature.

2.2 Nonpitaxial growth of poly-crystalline ZnO based TCOs on glass substrates

2.2.1 Fabrication of IMC buffer layers on glass substrates

IMC buffer layers were deposited onto quartz glass substrates by RF magnetron sputtering. The target-substrate distance was 100 mm. ZnO ceramic targets (2 inch in diameter) were used, and the RF power supplied to each target was 50 W. The substrate temperature was 300°C. Ar-N_2 mixed gas with an N_2/(Ar+N_2) flow rate ratio of 0.20 was used, and the total deposition pressure was 0.45 Pa. For the study of desorption behavior of nitrogen from films, Ar-N_2 mixed gas with N_2/(Ar+N_2) = 0.65 was employed, since nitrogen in IMC buffer layers fabricated under the above mentioned condition could not be detected by our XRF system (Rigaku ZSX Primus II) . The film thickness was varied from 1 to 100 nm. For comparison, ZnO buffer layers were prepared by in pure Ar atmosphere with the same sputtering system ("conventional buffer layers").

2.2.2 Fabrication of poly-crystalline AZO films on IMC buffer layers

AZO films were deposited on buffer layers as well as without buffer layers, with the same sputtering system as that used for buffer layer deposition. The target-substrate distance was 75 mm. ZnO:Al_2O_3 (2 wt.%) targets were used and the RF power supplied to each target was 130 W. The substrate temperature was 200°C. Pure Ar was used, and the working pressure was 0.34 Pa. AZO film thickness was 20-200 nm. The structural properties of the films were analyzed with XRD (Bruker D8 Discover) using Cu Kα radiation (λ= 0.154 nm). The film thickness of 10 to 100 nm-thick films was obtained by XRR method, whereas the thickness below 10 nm was an effective one deduced from the deposition rate. The surface

morphology of the films was characterized with AFM (Veeco Nanoscope II). The scanned surface area was 1×1 μm^2. AFM data was analyzed using an image processing software, ImageJ [16,17]. The electrical properties of AZO films were measured by Hall-effect measurement.

3. RESULTS AND DISCUSSION

3.1 Sputter deposition of single crystalline ZnO films on lattice mismatched substrates

3.1.1 Roles of impurity during fabrication of buffer layers on lattice mismatched substrates

AFM observation reveals that nitrogen introduced as impurities has significant effects on increase in the grain density as well as the surface smoothing of buffer layers fabricated on lattice mismatched substrates. Figures 1(a) and (b) show AFM images of a conventional buffer layer fabricated in Ar-O_2 atmosphere and an IMC buffer layer fabricated in Ar-N_2 atmosphere, respectively. During epitaxial growth of conventional buffer layers on sapphire substrates, highly strained two-dimensional (2D) layers are initially formed, and then subsequent growth of three-dimensional (3D) columnar grains on the 2D layers releases the strain energy stored in the films (Stranski–Krastanov mode) that comes from the large lattice mismatch of 18%. As a result, conventional buffer layers have grains with poor crystal-axis alignment and rough surfaces. Figure 1 (c) shows XRD phi scan of (101) plane for a conventional buffer layer, indicating large twist angle as well as the presence of 30°-rotated domains. The root-mean-square (RMS) roughness of the conventional buffer layer, derived from the analysis of AFM image, is large of 0.83nm. In contrast, our IMC buffer layer possesses high surface concentration of crystal grains, attributed to the adsorbed nitrogen atoms that disturb lateral growth of crystal grains. Owing to the small grain size, the strain energy is s efficiently released at grain boundaries even at the early stage of crystal growth, resulting in the films with small twist angle without a rotated domain (Fig. 1 (d)). Furthermore, the RMS roughness is drastically reduced to 0.14 nm.

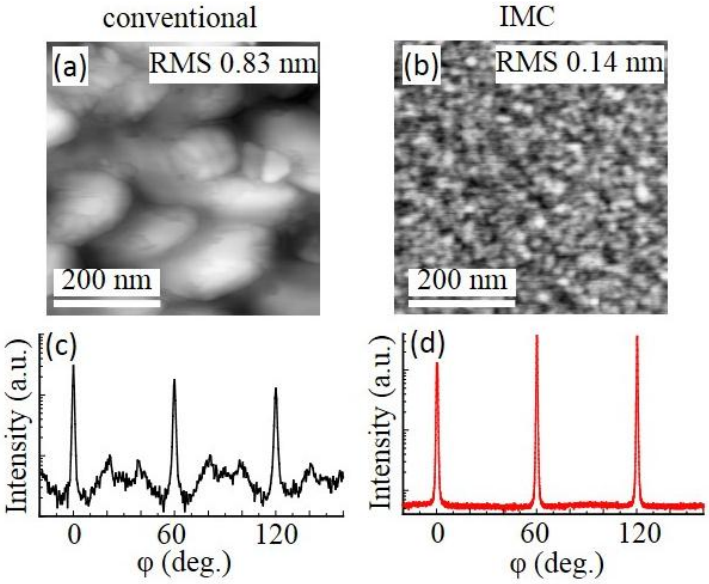

Figure 1. (a), (b) AFM images of conventional buffer layer (a) and IMC buffer layers (b). **(c)**, **(d)** XRD phi scans of ZnO (101) planes for conventional buffer layer (c) and IMC buffer layer (d). The film thickness is 10 nm.

3.1.2 Substrate-temperature effects on the morphology of IMC buffer layers

Next, we investigated the effects of substrate temperature T_s, which governs nitrogen desorption behaviour during film growth, on the morphology of buffer layers. Figure 2 shows the deposition rates of IMC buffer layers as a parameter of T_s. For a comparison, deposition rates of conventional buffer layers

are also shown in Fig. 2. With increasing T_s, the deposition rate of conventional buffer layer monotonically decreases, attributed to the enhancement in the desorption of Zn and O atoms from the growth surface. In contrast, the deposition rate of IMC buffer layer shows somewhat complicated behaviour. The lower deposition rate of IMC buffers in the whole T_s range is interpreted as the result of nitrogen atoms inhibiting the crystal growth of ZnO. In T_s range 680–720°C and 735–780 °C, the deposition rate of IMC buffer layer decreases with increasing T_s as is the case with ZnO films. On the other hand, in T_s range 720–735°C, the deposition rate increases with increasing T_s. These results suggest that the lifetime of adsorbed nitrogen atoms that disrupt the crystal growth as well as enhance the migration of adatoms such as Zn and O is significantly decreases with increasing T_s from 720°C to 735°C.

Figure 3 shows grain density of IMC-ZnO buffer layers as a parameter of T_s. The grain density of IMC buffer layer increases with increasing T_s from 700 to 735°C, attributed to the enhancement in the migration of adsorbed nitrogen that disrupt the crystal growth. A further increase in T_s, however, decreases the grain density. This decrease results from the fact that the crystal grains of IMC buffer layers become larger and are distributed more sparsely in T_s range 735–780°C. This morphology change observed at T_s >735°C is because of the short lifetime of the nitrogen adatoms at high T_s. Figure 4 shows height distributions of IMC buffer layers fabricated at various T_s, which are derived from AFM images. As T_s increases from 700 to 735°C, the height distribution becomes narrower, and the peak width reaches minimum at T_s=735°C, where the crystal grains are distributed densely and homogeneously. While, as T_s increases from 735 to 780°C, the height distribution become broader, which is due to inhomogeneous nucleation resulting from the large desorption rate of nitrogen adatoms from the growth surface.

Figure 2. (a) Deposition rate of buffer layers as a parameter of T_s. (b) Grain density of IMC buffer layers as a parameter of T_s. (c) Height distributions of IMC buffer layers fabricated at various T_s.

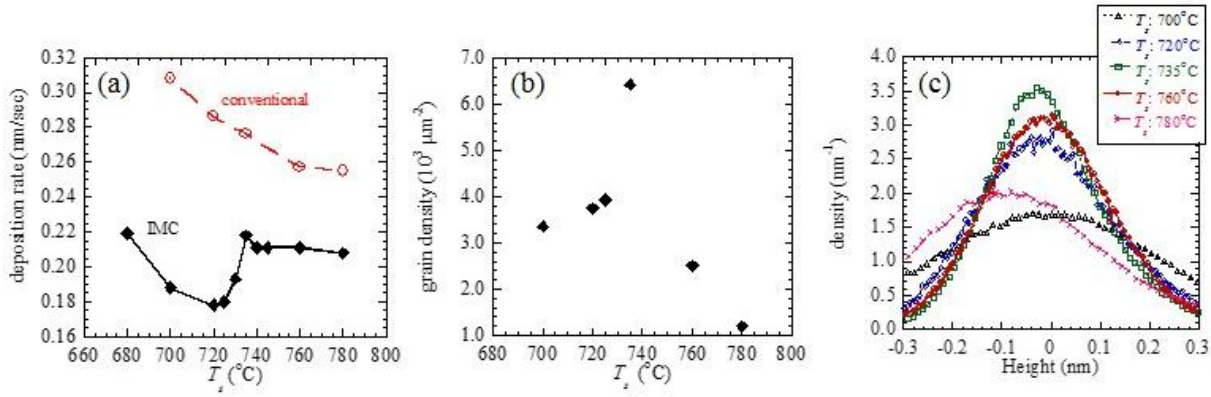

3.1.3 Growth of single crystalline ZnO films on IMC buffer layers

By utilizing IMC buffer layers, single crystalline ZnO films on lattice-mismatched c-Al_2O_3 substrates (18%) have been successfully fabricated. Figures 3 (a) and (b) show AFM images of ZnO films fabricated on a conventional buffer l the films were annealed at 1000°C for 3 hours in air. ystalline ZnO film that has atomically-flat surface wit c-axis length of ZnO. Full width at half maximum (F and (10-11) plane are 47 arcsec and 335 arcsec, t ZnO films fabricated on conventional buffer layers.

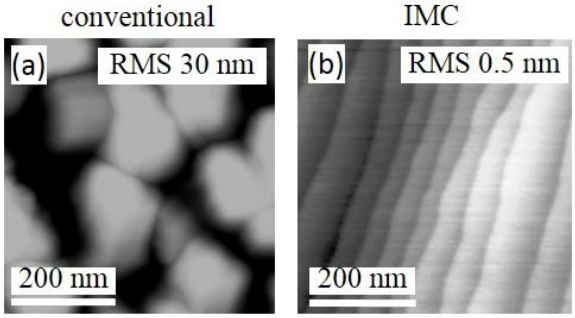

Figure 3. AFM images of ZnO films fabricated on a conventional buffer layer (a) and on IMC buffer layer (b).

3.1.4 Effects of surface morphology of IMC buffer layers on crystal growth of ZnO growth

Aiming at further improvement of the quality of ZnO films, we have studied effects of the surface morphology of IMC buffer layers on the crystal growth of ZnO. Figure 4 shows AFM images of ZnO films grown on IMC buffer layers that were deposited at various T_s. Here, all the ZnO films were fabricated at 700°C, and no post annealing was performed. It was fond that the morphology of the buffer layers significantly affects the crystal growth of ZnO. On IMC buffer layer fabricated at T_s=735°C, a pit-free ZnO single crystal with atomically-flat surface is grown. Since the buffer layer fabricated at T_s=735°C has the smoothest surface with RMS roughness of 0.128 nm, which owes to the densely and homogeneously distributed crystal grains, the enhanced migration of adsorbed Zn and O atoms on the buffer layer may result in the lateral growth of ZnO crystal. In contrast, poly-crystalline ZnO film with large roughness is grown on the buffer layer fabricated at T_s= 780°C, the mechanism of which is discussed below.

Figure 5 shows FWHM of (0002) symmetric rocking curves for ZnO films on IMC buffer layers as a function of the substrate temperature T_s for buffer layer deposition. Here, all the ZnO films are epitaxially grown on c-sapphire substrates, where the epitaxial relationship between ZnO and sapphire is $[0001]_{ZnO}$ $\|[0001]_{sapphire}$ and $[10\text{-}10]_{ZnO}$ $\|[11\text{-}20]_{sapphire}$. ZnO films with high out-of-plane alignment are obtained by using IMC buffer layers fabricated at T_s=700-760°C. While, on IMC buffer layer fabricated **Figure 4.**

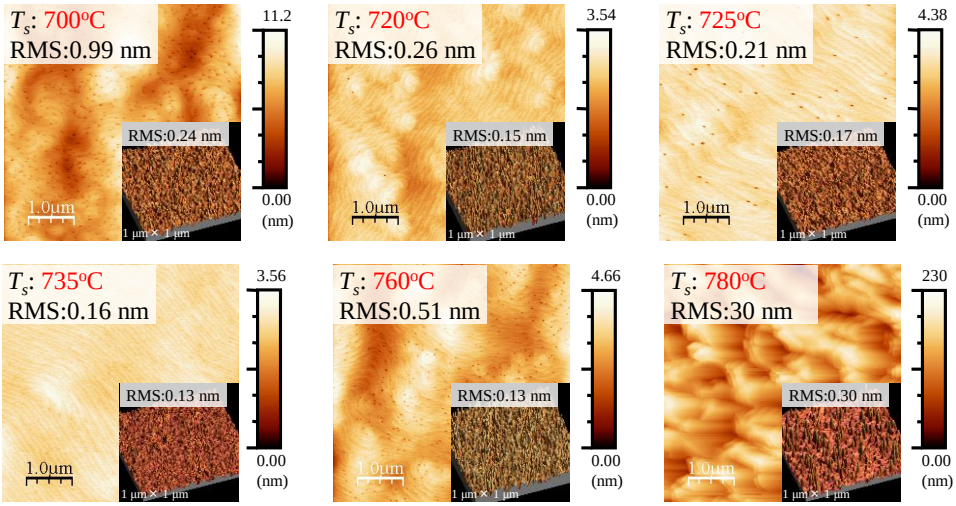

AFM images of ZnO films deposited on IMC buffer layers that were fabricated at 700°C (a), 720°C (b), 725°C (c), 735°C (d), 760°C (e), and 780°C (f). Here, no post annealing was performed. Inset shows AFM images of IMC buffer layers.

at T_s=780°C, ZnO film has large tilt angle, resulting in the large FWHM of 0.26°. From the analysis of residual stresses of ZnO films by using Williamson-Hall method [18], the good out-of-plane alignment observed at T_s = 700-760°C was found to be due to the small residual stress of ZnO films. In the case of epitaxial growth on lattice mismatched substrates, large strain energy is generally stored in the films as is

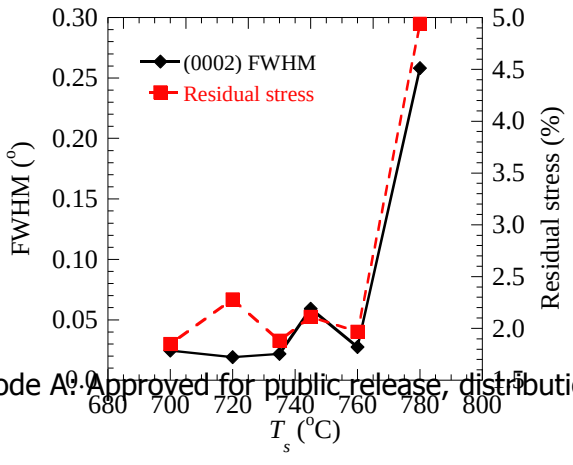

the case when using the buffer layer fabricated at T_s=780°C. However, by utilizing the buffer layers with large grain density obtained at T_s=700-760°C, the strain energy is efficiently released at grain boundaries, resulting in the films with low residual stress, that is, the films with good alignment in the crystal axis.

Figure 5. FWHM of (0002) symmetric rocking curves and residual stress of ZnO films versus substrate temperature Ts for buffer layer deposition.

3.1.5 Growth model of single crystalline ZnO films fabricated on IMC buffer layers

Based on the above results, we propose a growth model of single crystalline ZnO films that are prepared on lattice-mismatched sapphire substrates with IMC buffer layers, the schematic of which is shown in Fig. 6. On conventional buffer layers, the large surface roughness of buffer layers does not allow 2D growth, and the large tilt and twist angles prevent coalescence of columnar grains. In contrast,

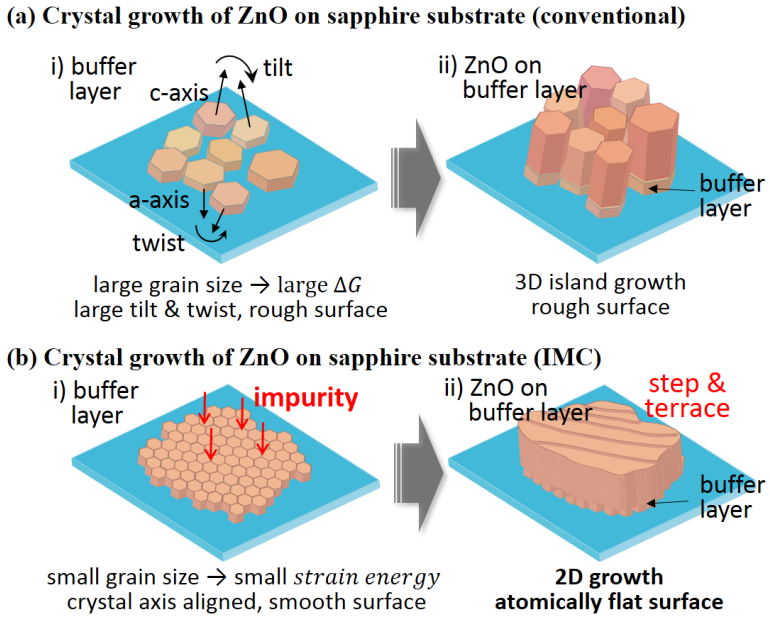

Figure 6. Crystal growth model of ZnO on lattice-mismatched substrates.

on IMC buffer layers, 3D columnar grains are initially formed, and then subsequent coalescence of the grains occurs because all of the grains are well aligned in both out-of-plane and in-plane directions. The smooth surface of IMC buffer layers also enhance the migration of adatoms, which allows 2D crystal growth of ZnO films, resulting in single crystalline ZnO with atomically flat surface. Since the concept of this crystal growth method can be applied to other materials that have no lattice-matched substrates, IMC-method will also open up a new pathway for development of wide variety of materials.

3.2 Sputter deposition of poly-crystalline ZnO based TCOs on glass substrates

3.2.1 Roles of impurity during non-epitaxial growth on glass substrates

3.2.1.1 Impurity concentration in IMC buffer layers

IMC method is a method in which the nitrogen atoms introduced as impurity are used to control nucleation via impurity adsorption and desorption. Therefore, it is of importance to study the nitrogen desorption behaviour as well as to evaluate the amount of residual nitrogen in the films. For this purpose, we measured nitrogen concentration in IMC buffer layers deposited at various temperature by XRF. The results are shown in Figure 7. Here $N_2/(Ar+N_2)$ flow rate ratio was 0.65. Nitrogen concentration at RT and 100°C is around 15 at.%. It decreases down to 2.5 at.% with increasing the temperature up to 500°C. XRD wide scan reveals that no Zn_3N_2 is formed, and all films in this study are ZnO. Moreover, nitrogen is a very insoluble element in ZnO, that is, the solubility limit of nitrogen in ZnO is 4 atomic ppm [19]. The solute element, nitrogen can either take a substitutional position or an interstitial position of ZnO crystals. Since our films are polycrystalline ones, probably being more defective than those in [19], more grain boundaries and vacancies in films can trap nitrogen, making the nitrogen solubility of our films higher than 4 atomic ppm. Moreover nitrogen concentration in films tend to be higher for films deposited at the lower deposition temperature, because crystallinity degrades and nitrogen desorption from surface is suppressed. We deduced that activation energy of nitrogen desorption from IMC ZnO buffer layers is 0.19 eV. This activation energy of nitrogen desorption is much lower than that of activation energy of desorption of chemisorbed hydrogen from ZnO (0.47-0.81 eV) [20], indicating that the nitrogen is easily desorbed out from films. IMC buffer layers hereafter were deposited at 300°C using Ar-N_2 mixed gas of $N_2/(Ar+N_2)$ flow rate ratio of 0.20, and hence N concentration in the films is below the detection limit of XRF.

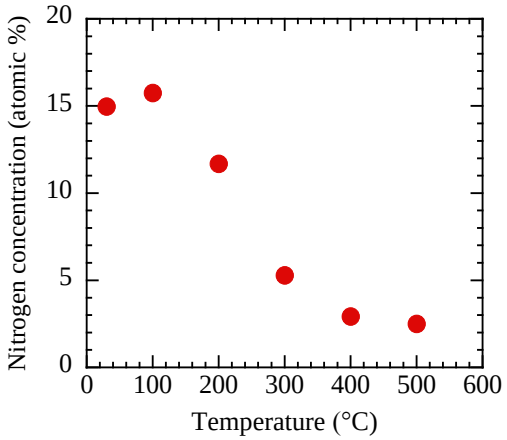

Figure 7. Deposition temperature dependence of N concentration in IMC buffer layers. $N_2/(Ar+N_2)$ flow rate ratio was 0.65.

3.2.1.2 Evolution of surface morphology of IMC buffer layers

Evolution of surface morphology of IMC and conventional buffer layers was observed by AFM. Figure 8 shows AFM images of buffer layers as a parameter of the film thickness. It is worthy for noting that nucleation takes place densely and uniformly at IMC-buffer-layer thickness of 4 nm. Further increase in the film thickness gives similar surface morphology except an increase in the grain size. At the early growth stage of 3 nm in thickness, the conventional buffer layer has less uniform surface morphology with sparsely distributed grains. Then the buffer layer keeps its less uniform surface morphology with inhomogeneously distributed grains.

Figure 9 shows average grain size of buffer layers deduced from AFM images. The grain size of conventional buffer layer monotonically increases with the film thickness, indicating the crystal grains grow in a similar way in the entire thickness region. On the other hand, grain growth of IMC

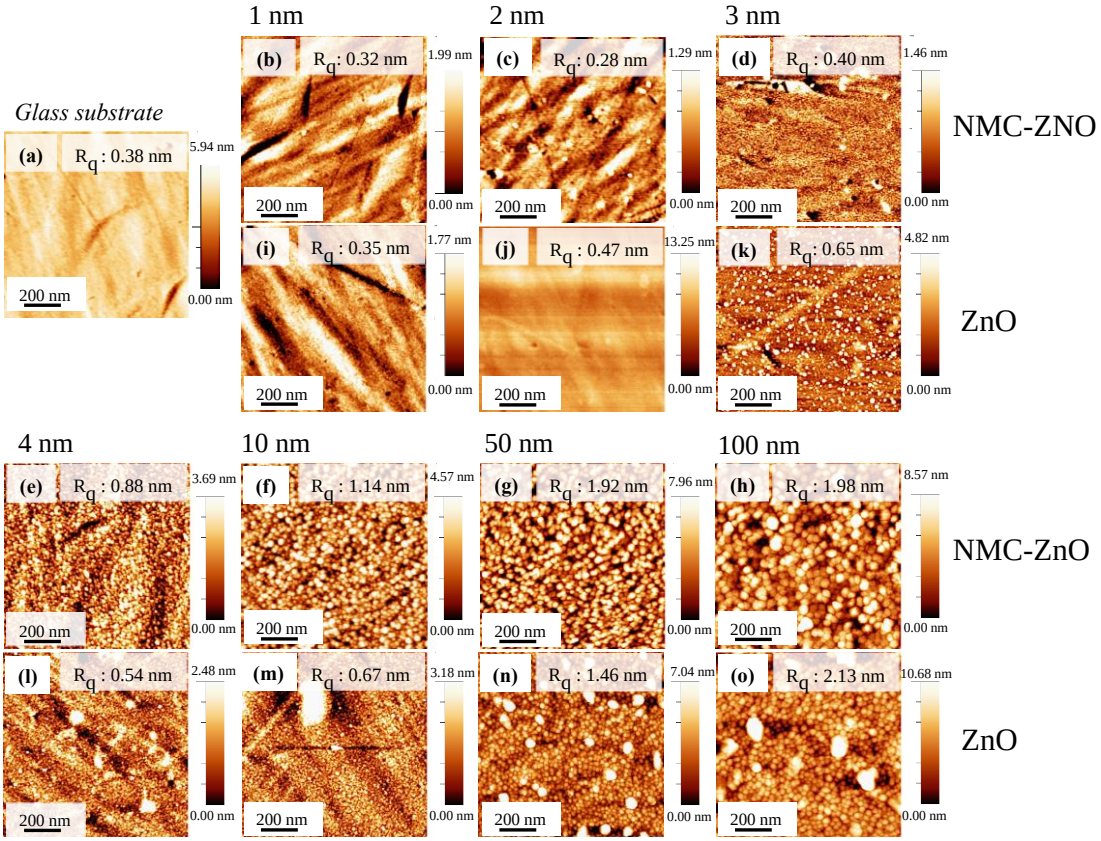

Figure 8. AFM images of IMC buffer layers (b)-(h) and conventional buffer layers (i)-(o) for film thickness of 1, 2, 3, 4, 10, 50, 100 nm. R_q represents the RMS roughness of the films.

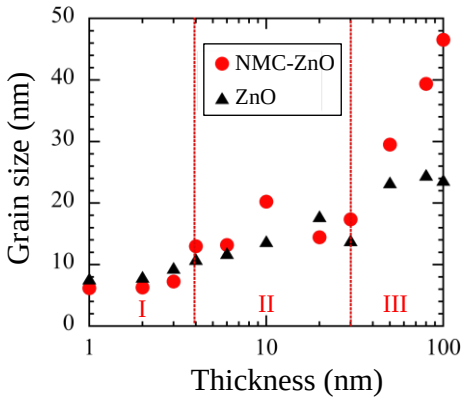

Figure 9. Film thickness dependence of average grain size of IMC and conventional buffer layers.

buffer layer can be classified into three stages: stage I of 1-3 nm in thickness, stage II of 4-30 nm in thickness, and stage III of 31-100 nm in thickness. In the stage I, the average grain size is a nearly constant of 7 nm because of little nucleation. In the stage II, the average grain size jumps to 13 nm at a threshold thickness of 4 nm and then it increases to 17 nm at 30 nm in thickness. In the stage III, grains grow fast to 47 nm at 100 nm in thickness. In the stages II and III, the average grain size of IMC buffer layers is larger than that of conventional buffer layers.

Figures 10(a), (b) and (c), (d) display the grain size distribution of IMC and conventional buffer layers as a parameter of the film thickness. For IMC buffer layers of 1-3 nm in thickness, the distributions are close to that of a glass substrate, again suggesting little nucleation. When the thickness increases from 3 to 4 nm, there is a notable change in the distribution, because nucleation takes place at 4 nm. The most important difference between the grain size distribution of IMC buffer layers and conventional buffer layers is that the number density of small grains for IMC buffer decreases considerably with increasing the film thickness, whereas that for conventional buffer remains high even at 100 nm. From these results, we can conclude that nucleation of IMC buffer layers takes place in a very short period, and Zn and O atoms impinging on the surface mainly contribute to grain growth after the period. This feature of IMC buffer layers is the key for obtaining high-quality ZnO based TCOs deposited on IMC buffer layers.

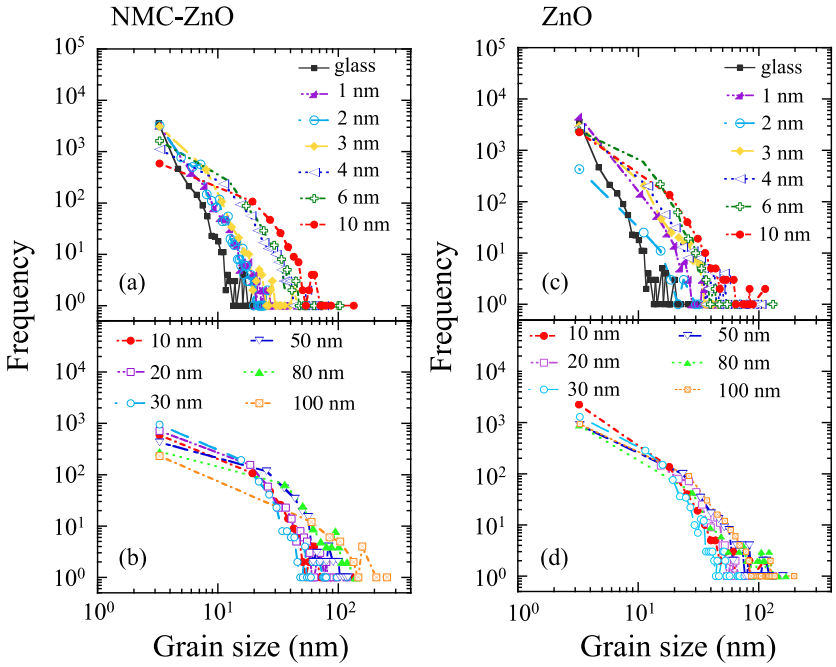

Figure 10. Grain size distribution of NMC-ZnO (a), (b) and ZnO (c), (d) as a parameter of film thickness. Characteristic lateral size distribution of glass substrate is also shown in (a) and (c) for comparison.

3.2.1.3 Lateral correlation length of IMC buffer layers

The lateral correlation length ξ, which provides a measure of the surface diffusion length, were deduced form the height-height correlation function (HHCF) analysis [21-23]. Figure 11 shows HHCF of IMC and conventional buffer layers, indicating that introduction of nitrogen increases the lateral correlation length ξ of ZnO films, that is, migration of adatoms at the growth surface is enhanced by IMC method. Here the films thickness of buffer layers is 10 nm. Such surface migration allows adatoms to reach the lowest thermodynamically favored lattice positions, and therefore, the crystal grain size becomes larger and the crystallinity of the films improves as described in the next section.

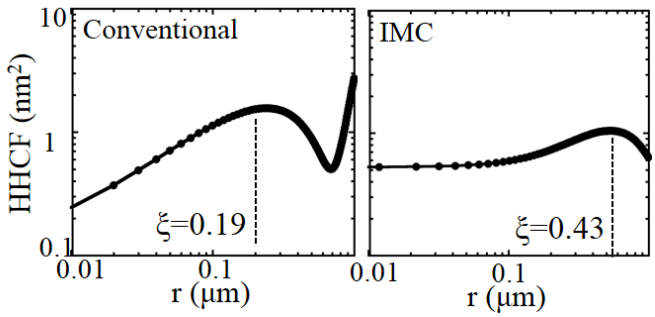

Figure 11. Height-height correlation function (HHCF) of conventional and IMC buffer layers. Here the films thickness was 10 nm.

3.2.1.4 Crystallographic characteristics of IMC buffer layers

Figure 12 shows the x-ray diffraction patterns of IMC buffer layers. XRD wide scan (Fig. 12 (b)) shows no peak apart from (0002) peaks around 34° and (0004) peaks around 72°, indicating an oriented growth along the *c*-axis perpendicularly to the substrate surface. This is also a clear evidence that there is no antibixbyite Zn_3N_2 and only ZnO phase presents in the film. With increasing the film thickness from 10 to 100 nm, FWHM becomes narrower associated with a larger grain size of the film. The grain size deduced from FWHM increases from 10.37 nm for 10 nm in thickness to 30.26 nm for 100 nm in thickness. Figures 12 (c) and (d) show 2θ-ω scans and rocking curves of ZnO (0002) plane. FWHM of 2θ-ω scan for IMC buffer layer is narrower than that for conventional buffer layer, associated with a larger grain size of IMC buffer layers, the results of which are in good agreement with the average grain size derived from AFM images shown in Figure 9. FWHM of rocking curve for IMC buffer layer is also smaller than that for conventional buffer, indicating that IMC buffer has better out-of- plane crystal alignment.

3.2.1.5. Growth mechanism of IMC buffer layers non-epitaxially grown on glass substrates

Based on the aforementioned investigation, we propose a growth mechanism of IMC buffer layers on glass substrates. The growth of IMC buffer layers is classified into three stages, that is, stage I of pre-nucleation, stage II of nucleation and grain growth for 4-30 nm in thickness, and stage III of coalescence for 31-100 nm in thickness. In plasma, nitrogen atoms are generated through electron impact dissociation of N_2 or charge exchange between N_2 and Ar^+ followed by dissociative recombination of N_2^+ [24,25]. Therefore nitrogen as well as Zn and O impinge on the substrate surface. Among these impinging species, Zn and O tend to deposit as ZnO on the surface, whereas nitrogen atoms are adsorbed and migrate on the surface and are eventually desorbed from the surface. At the early stage of the growth, Zn and O on the substrate surface may collide with each other to join into small clusters, then some clusters grow to large ones. Such large clusters are not in a stable state before overcoming a nucleation energy barrier ΔG^* to reach a critical radius for nucleation. Nitrogen atoms, "impurities", tend to suppress nucleation of ZnO, when they are adsorbed onto the surface of clusters and/or the substrate surface as shown in the stage I for the film thickness from 1 to 3 nm [26]. Thus nitrogen atoms increase the nucleation energy barrier, the critical radius for nucleation, and the critical concentration of adatoms on the surface for nucleation. Additional doses of Zn and O impinging on the substrate bring the concentration of adatoms on the surface above the critical concentration for nucleation, leading to spatially uniform nucleation for the film thickness of 4 nm. After nucleation takes place in a very short period, nucleation ceases; because adatoms on the surface are preferentially adsorbed to nuclei growing to grains and the concentration of adatoms on the surface becomes below the critical concentration for nucleation in the stage II. This nucleation in a very

short period brings grains with rather uniform size and hence flat surface. The growing grains then start to collide with each other and coalesce to form a continuous polycrystalline film with a large grain size in the stage III.

In the case of conventional buffer layers, the nucleation energy barrier ΔG^* is low and hence nucleation takes place even at low temperature <100°C [27]. Therefore, at 300°C in this study, nucleation takes place even for very low dose of Zn and O. Because the size of nuclei is very small due to the low nucleation energy barrier; this nucleation at the very early stage is difficult to be clearly distinguished in AFM images. Then such small nuclei grow to grains by absorbing some adatoms on the substrate surface and such grains are appreciable in Figure 8 (k), whereas other adatoms still contribute to new nucleation because the critical concentration for nucleation is low compared with IMC buffer layers. Therefore the nucleation period of conventional ZnO is long compared with IMC buffers. This successive nucleation in the nucleation stage brings about less uniform spatial distribution of grains with a wide size range. As a result a polycrystalline film with a rather wide crystal grain size range is formed.

3.2.2 Fabrication of low-resistive AZO films on IMC buffer layers

By utilizing IMC buffer layers, AZO films with high crystal quality have been obtained. For AZO films on 10-nm-thick IMC buffer layers, FWHM of XRD 2θ-ω scan of (0002) plane is about 0.2°, whereas the FWHM for AZO films without buffer layer is 0.4-0.6°, depending on the deposition conditions. Here the thickness of AZO films is 100 nm. Furthermore, by utilizing IMC buffer layers, AZO films with low resistivity have been obtained. Figure 12 shows the resistivity of AZO films prepared on IMC buffer layers as a function of AZO film thickness. The most remarkable effect of IMC buffer layers is a significant reduction in the resistivity for the films thinner than 100 nm. The resistivity of AZO films fabricated by a conventional sputtering increases substantially from 6.3×10^{-4} to 1.5×10^{-3} Ω·cm with decreasing the film thickness from 200 nm to 20 nm, while the resistivity of AZO films with IMC buffer layers is low of $2.8\text{-}3.2\times10^{-4}$ Ω·cm in the thickness range 20-200 nm. In the case of conventional sputtering, the excessive nucleation with various orientations is induced by high energy of impingement of the sputtered species and/or the fragments from plasma at the initial stage of the deposition. As the film grows, the films are gradually dominated by c-axis orientation due to the large anisotropic surface energy and large growth rate along c axis of wurtzite structure. Therefore, the crystallinity of the conventional AZO films changes much with the film thickness, which has been confirmed by XRD analysis. This is one of the reason why the resistivity increases much with decreasing the film thickness in the case of conventional sputtering. On the other hand, on IMC buffer layers, AZO films with high crystallinity are grown from the early stage of deposition, owing to the high crystal quality of IMC buffer layers. As a result, the crystallinity of AZO films deposited on IMC buffer layers does not change **Figure 12.** Resistivity

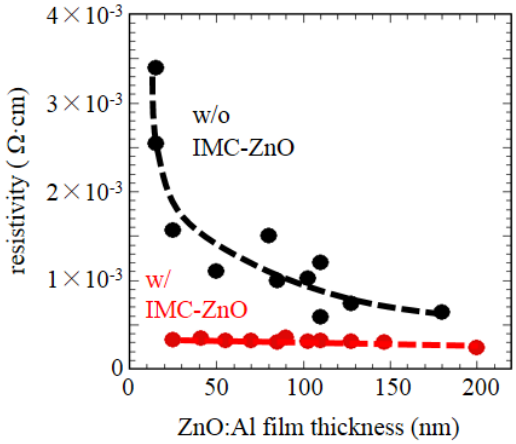

of AZO films prepared with and without IMC buffer layers as a function of AZO film thickness. The buffer layer thickness is 10 nm.

with the film thickness, and low resistivity is observed even for the films with small thickness. For instance, at the thickness of 20 nm, the resistivity of AZO films prepared by a conventional method is 1.5×10^{-3} Ω·cm, whereas the resistivity of AZO films prepared on the buffer layers is 3.2×10^{-4} Ω·cm that is even smaller than that of AZO films fabricated by pulsed-laser deposition (PLD) [1].

3.2.3 Electrical analysis of AZO films on IMC buffer layers

Research collaborator: Professor David C. Look, Write State University, The United States.

In order to further discuss the effects of IMC buffer layers especially on the electrical properties of AZO films, collaborative research with Prof. David C. Look of Write State University has been performed. He examined the buffer effects by calculating the electrical thickness d_{el} of AZO films, which is different than the metallurgical thickness *d*, bulk donor and acceptor concentrations, and new figure of merit *d** to describe interface quality [28]. He found that the volume carrier concentration *n* of AZO films is independent of the thickness *d* over the thickness range 25-147 nm, and *n* is also not affected by the presence of IMC buffer layers. However, the mobility is strongly influenced by IMC buffer layers, exhibiting independence from AZO film thickness and increased magnitude at a given thickness of AZO films. Theoretical analysis shows that the observed lower mobility in thinner AZO layers, especially in those without a buffer, is due to increased scattering at the interface because the electrons are closer to it. The effect of IMC buffer layers is to reduce this scattering and also to reduce or eliminate the trapping at the interface of free electrons from the bulk.

4. SUMMARY

In this research, a fabrication method of ZnO based on magnetron sputtering, "impurity-mediated crystallization (IMC)", has been developed, where crystal nucleation and growth are controlled by adsorbed impurities on the growth surface. The crystal growth mechanism of ZnO prepared by IMC method has been clarified by observation of the morphology evolution during film growth of both epitaxial and non-epitaxial ZnO films. Utilizing the IMC films as buffer layers, two kinds of high quality ZnO films have been fabricated. One is single crystalline ZnO films on lattice-mismatched c-plane sapphire substrates for LED and LD applications, and the other is very low resistive ZnO:Al films on glass substrates for TCO applications. The high quality ZnO films obtained by IMC method will lead to replacement of rare-metal-based materials such as GaN and In_2O_3:Sn in optoelectronic devices, bringing significant reduction in the cost as well as the damage to human health and the environment. Since the application of IMC method is not limited to ZnO, this method will not only accelerate the practical use of ZnO in optoelectronic devices but also open up a new pathway for development of other oxide materials that have no cost-effective lattice-matched substrates.

REFERENCES

[1] T. Minami, T. Miyata, *Thin Solid Films*, **517**, 1474 (2008).

[2] T. Amamoto, T. Shiosaki, A. Kawabata, *J. Appl. Phys.*, **51**, 3113 (1980).

[3] U. Ozgur, Y. Alivov, C. Liu, A. Teke, M. Reshchikov, S. Dogan, V. Avrutin, S. Cho, H. Morkoc, *J. Appl. Phys.*, **98**, 041301 (2005).

[4] J. Jia, A. Takasaki, N. Oka, Y. Shigesato, *J. Appl. Phys.*, **112**, 013718 (2012).

[5] F. Ruske, M. Roczen, K. Lee, M. Wimmer, S. Gall, J. Huepkes, D. Hrunski, B. Rech, *J. Appl. Phys.*, **107**, 013708 (2010).
[6] N. Itagaki, K. Kuwahara, K. Nakahara, D. Yamashita, G. Uchida, K. Koga, M. Shiratani, *Appl. Phys. Express*, **4**, 011101 (2011).
[7] Y. Imanishi, M. Taguchi, K. Onisawa, *Thin Solid Films*, **518**, 2945 (2010).
[8] K. Nakahara, S. Akasaka, H. Yuji, K. Tamura, T. Fujii, Y. Nishimoto, D. Takamizu, A. Sasaki, T. Tanabe, H. Takasu, H. Amaike, T. Onuma, S.F. Chichibu, A. Tsukazaki, A. Ohtomo, M. Kawasaki, *Appl. Phys. Lett.*, **97**, 013501 (2010).
[9] A. Tsukazaki, A. Ohtomo, T. Onuma, M. Ohtani, T. Makino, M. Sumiya, K. Ohtani, S. Chichibu, S. Fuke, Y. Segawa, H. Ohno, H. Koinuma, M. Kawasaki, *Nature Materials*, **4**, 42 (2005).
[10] D.C. Look, B. Claflin, Y.I. Alivov, S.J. Park, *Phys. Status Solidi A*, **201**, 2203 (2004).
[11] P. Fons, K. Iwata, S. Niki, A. Yamada, K. Matsubara, *J. Cryst. Growth*, **201**, 627 (1999).
[12] V. Khranovskyy, R. Minikayev, S. Trushkin, G. Lashkarev, V. Lazorenko, U. Grossner, W. Paszkowicz, A. Suchocki, B.G. Svensson, R. Yakimova, *J. Cryst. Growth*, **308**, 93 (2007).
[13] T. Nakamura, Y. Yamada, T. Kusumori, H. Minoura, H. Muto, *Thin Solid Films*, **411**, 60 (2002).
[14] H. Amano, N. Sawaki, I. Akasaki, Y. Toyoda, *Appl. Phys. Lett.*, **48**, 353 (1986).
[15] M. Sumiya, A. Tsukazaki, S. Fuke, A. Ohtomo, H. Koinuma, M. Kawasaki, *Appl. Surf. Sci.*, **223**, 206 (2004).
[16] Y. Yamazaki, R. Hernandez-Sanchez, S.M. Haile, *Chemistry of Materials*, **21**, 2755 (2009).
[17] I. Suhariadi, K. Matsushima, K. Kuwahara, K. Oshikawa, D. Yamashita, H. Seo, G. Uchida, K. Kamataki, K. Koga, M. Shiratani, S. Bornholdt, H. Kersten, H. Wulff, N. Itagaki, *Jpn. J. Appl. Phys.*, **52**, 11NB03 (2013).
[18] G. WILLIAMSON, W. HALL, *Acta Metallurgica*, **1**, 22 (1953).
[19] M. Komatsu, N. Ohashi, I. Sakaguchi, S. Hishita, H. Haneda, *Appl. Surf. Sci.*, **189**, 349 (2002).
[20] M. Watanabe, *J. Res. Inst. Catalysis*, **26**, 63 (1978).
[21] Z. Liu, N. Jiang, Y. Shen, Y. Mai, *J. Appl. Phys.*, **92**, 3559 (2002).
[22] K. Bray, G. Parsons, *Physical Review B*, **65**, 035311 (2002).
[23] H. Yang, Y. Zhao, A. Chan, T. Lu, G. Wang, *Phys. Rev. B*, **56**, 4224 (1997).
[24] S. Tada, S. Takashima, M. Ito, M. Hori, T. Goto, Y. Sakamoto, *J. Appl. Phys.*, **88**, 1756 (2000).
[25] T. Czerwiec, F. Greer, D. Graves, *Journal of Physics D-Applied Physics*, **38**, 4278 (2005).
[26] X. Liu, *J Phys Chem B*, **105**, 11550 (2001).
[27] A. Banerjee, C. Ghosh, K. Chattopadhyay, H. Minoura, A. Sarkar, A. Akiba, A. Kamiya, T. Endo, *Thin Solid Films*, **496**, 112 (2006).
[28] D.C. Look, K.D. Leedy, A. Kiefer, B. Claflin, N. Itagaki, K. Matsushima, I. Surhariadi, *Opt. Eng.*, **52**, 033801 (2013).

APPENDIX

PUBLICATIONS

i) Journal papers

1. "Synthesis and characterization of ZnInON semiconductor: a ZnO-based compound with tuneable band gap", **N. Itagaki**, K. Matsushima, D. Yamashita, H. Seo, K. Koga, M. Shiratani, ***Mater. Res. Express* 1** (2014) 036405.
2. "Growth mechanism of ZnO deposited by nitrogen mediated crystallization", I. Suhariadi, M. Shiratani, **N. Itagaki**, ***Mater. Res. Express* 1** (2014) 036403.
3. "Off-axis sputter deposition of ZnO films on c-sapphire substrates by utilizing nitrogen-mediated crystallization method" , **N. Itagaki**, K. Kuwahara, K. Matsushima, D. Yamashita, H. Seo, K. Koga, M. Shiratani, ***Opt. Engineering* 53** (2014) 087109.
4. "Infrared Plasmonics via ZnO", J.W. Allen, M.S. Allen, D.C. Look, B.R. Wenner, **N. Itagaki**, K. Matsushima, I. Surhariadi, ***J. Nano Res***. **8** (2014) 109.
5. "Nanostructure control of Si and Ge quantum dots based solar cells using plasma processes", M. Shiratani, G. Uchida, H. Seo, D. Ichida, K. Koga, **N. Itagaki**, and K. Kamataki, ***Materials Science Forum*, 783-786** (2014) 2022.s
6. "Performance dependence of Si quantum dot-sensitized solar cells on counter electrode", H. Seo, D. Ichida, G. Uchida, **N. Itagaki**, K. Koga, M. Shiratani, ***Jpn. J. Appl. Phys.*, 53** (2014) 05FZ01.
7. "Electrochemical impedance analysis on the additional layers for the enhancement on the performance of dye-sensitized solar cell", H. Seo, M. Son, S. Park, M. Jeong, H. Kim, G. Uchida, **N. Itagaki,** K. Koga, M. Shiratani, ***Thin Solid Films* 554** (2014) 122.
8. "Analysis on the photovoltaic property of Si quantum dot-sensitized solar cells", H. Seo, D. Ichida, G. Uchida, K. Kamataki, **N. Itagaki**, K. Koga, M. Shiratani, ***Int. J. Precision Eng. Manuf.*, 15** (2014) 339.
9. "Theory for correlation between plasma fluctuation and fluctuation of nanoparticle growth in reactive plasmas", M. Shiratani, K. Koga, K. Kamataki, S. Iwashita, G. Uchida, H. Seo, and **N. Itagaki**, ***Jpn. J. Appl. Phys*. 53** (2014) 010201
10. "Effects of Nitrogen on Crystal Growth of Sputter-Deposited ZnO Films for Transparent Conducting Oxide", I. Suhariadi, K. Oshikawa, K. Kuwahara, K. Matsushima, D. Yamashita, G. Uchida, K. Koga, M. Shiratani, **N. Itagaki**, ***Jpn. J. Appl. Phys.* 52** (2013) 11NB03.
11. "Characteristics of Crystalline Silicon/Si Quantum Dot/Poly(3,4-ethylenedioxythiophene) Hybrid Solar Cells", G. Uchida, Y. Wang, D. Ichida, H. Seo, K. Kamataki, **N. Itagaki**, K. Koga, M. Shiratani, ***Jpn. J. Appl. Phys*. 52** (2013) 11NA05
12. "Correlation between Volume Fraction of Silicon Clusters in Amorphous Silicon Films and Optical Emission Properties of Si and SiH", Y. Kim, K. Hatozaki, Y. Hashimoto, G. Uchida, K. Kamataki, **N. Itagaki**, H. Seo, K. Koga, and M. Shiratani, ***Jpn. J. Appl. Phys*. 52** (2013) 11NA07.
13. "Flux Control of Carbon Nanoparticles Generated due to Interactions between Hydrogen Plasmas and Graphite Using DC-Biased Substrates", K. Koga, M. Tateishi, K. Nishiyama, G. Uchida, K. Kamataki, D. Yamashita, H. Seo, **N. Itagaki**, M. Shiratani, N. Ashikawa, S. Muzaki, K. Nishimura, Akiko Sagara, the LHD Experimental Group, ***Jpn. J. Appl. Phys*. 52** (2013) 11NA08.
14. "Improvement on the Electron Transfer of Dye-Sensitized Solar Cell Using Vanadium Doped TiO2", H. Seo, Y. Wang, D. Ichida, G. Uchida, **N. Itagaki**, K. Koga, M. Shiratani, S. Nam, J. Boo, ***Jpn. J. Appl. Phys*. 52** (2013) 11NM02.
15. "Epitaxial Growth of ZnInON Films with Tunable Band Gap from 1.7 eV to 3.3 eV on ZnO Templates", K. Matsushima, T. Hirose, K. Kuwahara, D. Yamashita, G. Uchida, H. Seo, K. Kamataki, K. Koga, M.

Shiratani, **N. Itagaki**, ***Jpn. J. Appl. Phys*. 52** (2013) 11NM06.

16. "The improvement on the performance of quantum dot-sensitized solar cells with functionalized Si," H. Seo, Y. Wang, M. Sato, G. Uchida, K. Koga, **N. Itagaki**, K. Kamataki, M. Shiratani, ***Thin Solid Films* 546** (2013) 284-288.
17. "Study on the Fabrication of Paint-Type Si Quantum Dot-Sensitized Solar Cells", H. Seo, M. Son, H. Kim, Y. Wang, G. Uchida, K. Kamataki, **N. Itagaki**, K. Koga, M. Shiratani, ***Jpn. J. Appl. Phys*. 57** (2013) 10MB07.
18. "Characteristics of Photocurrent Generation in the Near-Ultraviolet Region in Si Quantum-Dot Sensitized Solar Cells", G. Uchida, M. Sato, H. Seo, K. Kamataki, **N. Itagaki**, K. Koga, M. Shiratani, ***Thin Solid Films* 544** (2013) 93-98

ii) Conference papers

1. "Off-axis sputter deposition of ZnO films on c-sapphire substrates with buffer layers prepared via nitrogen-mediated crystallization", **N. Itagaki**, K. Matsushima, D. Yamashita, H. Seo, K. Koga, M. Shiratani, ***Proc. SPIE International Society for Optical Engineering*** 2014, **8987** (2014) 89871A
2. "Study on the Crystal Growth Mechanism of ZnO Films Fabricated Via Nitrogen Mediated Crystallization", I. Suhariadi, K. Oshikawa, D. Yamashita, K. Kamataki, G. Uchida, K. Koga, M. Shiratani, and **N. Itagaki**, ***Jpn. Phys. Soc. Conf. Proc. (APPC12)*, 1** (2014) 015064.
3. "Deposition of Carbon Films on PMMA Using H-assisted Plasma CVD", X. Dong, R. Torigoe, K. Koga, G. Uchida, M. Shiratani, **N. Itagaki**, Y. Setsuhara, K. Takenaka, M. Sekine, .M. Hori, ***J. Phys. : Conf. Series (APPC12)* 1** (2014) 015072.
4. "Effects of filter gap of cluster-eliminating filter on cluster eliminating efficiency", Y. Hashimoto, S. Toko, D. Yamashita, H. Seo, K. Kamataki, **N. Itagaki**, K. Koga and M. Shiratani, ***J. Phys. : Conf. Series (SPSM26)* 518** (2014) 012007.
5. "Contribution of ionic precursors to deposition rate of a-Si:H films fabricated by plasma CVD", S. Toko, Y. Hashimoto, Y. Kanemitu, Y. Torigoe, H. Seo, G. Uchida, K. Kamataki, **N. Itagaki**, K. Koga and M. Shiratani, ***J. Phys. : Conf. Series (SPSM26)* 518** (2014) 012008.
6. "Contribution of H2 plasma etching to radial profile of amount of dust particles in a divertor simulator", M. Tateishi, K. Koga, D. Yamashita, K. Kamataki, H. Seo, **N. Itagaki**, M. Shiratani, N. Ashikawa, S. Masuzaki, K. Nishimura and A. Sagara, the LHD Experimental Group, ***J. Phys. : Conf. Series (SPSM26)* 518** (2014) 012009.
7. "Emission spectroscopy of Ar + H2 + C7H8 plasmas: C7H8 flow rate dependence and pressure dependence", X. Dong, K. Koga, D. Yamashita, H. Seo, **N. Itagaki**, M. Shiratani, Y. Setsuhara, M. Sekine and M. Hori, ***J. Phys. : Conf. Series (SPSM26)* 518** (2014) 0120010.
8. "Plasma etching of single fine particle trapped in Ar plasma by optical tweezers", T. Ito, K. Koga, D. Yamashita, K. Kamataki, **N. Itagaki**, G. Uchida and M. Shiratani, ***J. Phys. : Conf. Series (SPSM26)* 518** (2014) 0120014.
9. "SiC Nanoparticle Composite Anode for Li-Ion Batteries", M. Shiratani, K. Kamataki, G. Uchida, K. Koga, H. Seo, **N. Itagaki**, T. Ishihara, ***Mat. Res. Soc. Symp. Proc.* 1678** (2014)
10. "Combinatorial Plasma CVD of Si Nanoparticle Composite Films for Band Gap Control", G. Uchida, Y. Kanemitsu, D. Ichida, H. Seo, K. Kamataki, **N. Itagaki**, K. Koga, M. Shiratani, ***Jpn. Phys. Soc. Conf. Proc (APPC12)* 1** (2014) 015080.
11. "Effects of H2 Gas Addition on Structure of Ge Nanoparticle Films Deposited by High-pressure RF Magnetron Sputtering Method", G. Uchida, D. Ichida, H. Seo, K. Kamataki, **N. Itagaki**, K. Koga, M. Shiratani, ***Jpn. Phys. Soc. Conf. Proc (APPC12)* 1** (2014) 015082.
12. "Correlation between nanoparticle growth and plasma parameters in low pressure reactive VHF

discharge plasmas", M. Shiratani, Y. Morita, K. Kamataki, H. Seo, G. Uchida, **N. Itagaki**, K. Koga, ***Jpn. Phys. Soc. Conf. Proc (APPC12)*** **1** (2014) 015083.

13. "Spatial Profile of Flux of Dust Particles Generated due to Interaction between Hydrogen Plasmas and Graphite Target", M. Tateishi, K. Koga, D. Yamashita, K. Kamataki, G. Uchida, H. Seo, **N. Itagaki**, M. Shiratani, N. Ashikawa, S. Masuzaki, K. Nishimura, A. Sagara, and the LHD Experimental Group, ***Jpn. Phys. Soc. Conf. Proc (APPC12)*** **1** (2014) 015020.
14. "Effects of Grid DC Bias on Incorporation of Si Clusters into Amorphous Silicon Thin Films in Multi-Hollow Discharge Plasma CVD", S. Toko, Y. Kim, Y. Hashimoto, Y. Kanemitu, H. Seo, G. Uchida, K. Kamataki, **N. Itagaki**, K. Koga, and M. Shiratani, ***Jpn. Phys. Soc. Conf. Proc (APPC12)*** **1** (2014) 015069.
15. "Coupling between radicals and nanoparticles in initial growth phase in reactive plasmas with amplitude modulation", K. Koga, Y. Morita1, K. Kamataki, D. Yamashita, **N. Itagaki**, G. Uchida, M. Shiratani, ***Proc. 8th Int. Conf. Reactive Plasmas*** (2014) 3B-WS-14.
16. "Epitaxial growth of ZnO films on sapphire substrates by magnetron sputtering: Effects of buffer layers prepared via nitrogen mediated crystallization", T. Ide, K. Matsushima, R. Shimizu, K. Koga, M. Shiratani, **N. Itagaki**, ***Proc. 8th Int. Conf. Reactive Plasmas*** (2014) 4P-PM-S08-P10.
17. "Quantum characterization and photovoltaic application of Si nano-particles fabricated by multi-hollow plasma discharge chemical vapor deposition", H. Seo, D. Ichida, G. Uchida, **N. Itagaki**, K. Koga, M. Shiratani, ***Proc. 8th Int. Conf. Reactive Plasmas*** (2014) 4P-PM-S11-P36.
18. "A model for correlation between plasma fluctuation and fluctuation of nanoparticle growth in reactive plasmas", M. Shiratani, K. Koga, K. Kamataki, S. Iwashita, Y. Morita, H. Seo, **N. Itagaki**, G. Uchida, ***Proc. 8th Int. Conf. Reactive Plasmas*** (2014) 4B-PM-O1.
19. "Fabrication of SiC nanoparticles as high capacity electrodes for Li-ion batteries", G. Uchida, K. Kamataki, D. Ichida, Y. Morita, H. Seo, **N. Itagaki**, K. Koga, T. Ishihara, M. Shiratani, ***Proc. 8th Int. Conf. Reactive Plasmas*** (2014) 4C-PM-O1.
20. "Analysis of fluctuation of Ar metastable density and nanoparticle amount in capacitively coupled discharges with amplitude modulation", Y. Morita, T. Ito, S. Iwashita, D. Yamashita, G. Uchida, H. Seo, K. Kamataki, **N. Itagaki**, K. Koga, M. Shiratani, ***Proc. 8th Int. Conf. Reactive Plasmas*** (2014) 5P-AM-S02-P10.
21. "Fine response of deposition rate of Si films deposited by multi-hollow discharge plasma CVD with amplitude modulation", S. Toko, Y. Hashimoto, Y. Kanemitu, Y. Torigoe, H. Seo, K. Kamataki, **N. Itagaki**, K. Koga, M. Shiratani, ***Proc. 8th Int. Conf. Reactive Plasmas*** (2014) 5P-AM-S05-P17.
22. "Spatial profile of flux of dust particles in hydrogen helicon plasmas", M. Tateishi, K. Koga, D. Yamashita, K. Kamataki, H. Seo, **N. Itagaki**, M. Shiratani, N. Ashikawa, S. Masuzaki, K. Nishimura, A. Sagara, the LHD Experimental Group, ***Proc. 8th Int. Conf. Reactive Plasmas*** (2014) 5P-AM-S05-P21.
23. "Raman spectroscopy of a fine particle optically trapped in plasma", D. Yamashita, K. Koga, G. Uchida, K. Kamataki, **N. Itagaki**, M. Shiratani, ***Proc. 8th Int. Conf. Reactive Plasmas*** (2014) 5P-AM-S05-P23.
24. "Subacute toxicity of gallium arsenide, indium arsenide and arsenic trioxide following intermittent intrantracheal instillations to the lung of rats", A. Tanaka, M. Hirata, K. Koga, **N. Itagaki**, M. Shiratani, N. Hayashi, G. Uchida, ***Proc. 8th Int. Conf. Reactive Plasmas*** (2014) 5P-AM-S12-P35.
25. "Nanoparticle amount in reactive plasmas with amplitude modulation detected by twodimensional laser light scattering method", T. Ito, Y. Morita, S. Iwashita, D. Yamashita, G. Uchida, H. Seo, K. Kamataki, **N. Itagaki**, K. Koga, M. Shiratani, ***Proc. 8th Int. Conf. Reactive Plasmas*** (2014) 5P-AM-SPD-P01.
26. "Fabrication of In-rich ZnInON filmswith narrow band gap by RF magnetron sputtering", K. Matsushima, R. Shimizu, T. Ide, D. Yamashita, G. Uchida, H. Seo, K. Kamataki, K. Koga, M. Shiratani, **N. Itagaki**, ***Proc. 8th Int. Conf. Reactive Plasmas*** (2014) 5P-PM-S08-P02.

27. "Sputtering fabrication of a novel widegap semiconductor ZnGaON for optoelectronic devices with wide bandgap for optical devices", R. Shimizu1, K. Matsushima, T. Ide, D. Yamashita, H. Seo, K. Koga, M. Shiratani, **N. Itagaki**, ***Proc. 8th Int. Conf. Reactive Plasmas*** (2014) 5P-PM-S08-P03.
28. "Study on nitrogen desorption behavior of sputtered ZnO for transparent conducting oxide", I. Suhariadi, K. Oshikawa, D. Yamashita, H. Seo, K. Koga, M. Shiratani, **N. Itagaki**, ***Proc. 8th Int. Conf. Reactive Plasmas*** (2014) 5P-PM-S08-P05.
29. "Magnetron sputtering of low-resistive In2O3:Sn films with buffer layers fabricated via nitrogen mediated crystallization", K. Oshikawa1, I. Suhariadi, D. Yamashita, H. Seo, K. Kamataki, G. Uchida, K. Koga, M. Shiratani, **N. Itagaki**, ***Proc. 8th Int. Conf. Reactive Plasmas*** (2014) 5P-PM-S08-P07.
30. "Pressure dependence of carbon film deposition using H-assisted plasma CVD", X. Dong, K. Koga, D. Yamashita, H. Seo, **N. Itagaki**, M. Shiratani, K. Takenaka, Y. Setsuhara, M. Sekine, M. Hori, ***Proc. 8th Int. Conf. Reactive Plasmas*** (2014) 5P-PM-S08-P14.
31. "Deposition of Crystalline Ge Nanoparticle Films Varying H2 Dilution Ratio Using High Pressure rf Magnetron Sputtering", S. Hashimoto, D. Ichida, G. Uchida, H. Seo, K. Kamataki, **N. Itagaki**, K. Koga, M. Shiratani, ***Proc. 8th Int. Conf. Reactive Plasmas*** (2014) 6P-AM-S08-P32.
32. "Fabrication of size-controlled Ge nanoparticle films varying gas flow rate using high pressure rf magnetron sputtering method", D. Ichida, S. Hashimoto, G. Uchida, H. Seo, D. Yamashita, K. Kamataki, **N. Itagaki**, K. Koga, M. Shiratani, ***Proc. 8th Int. Conf. Reactive Plasmas*** (2014) 6P-AM-S08-P33.
33. "Combinatorial evaluation of optical properties of crystalline Si nanoparticle embedded Si films deposited by a multi-hollow discharge plasma CVD method", Y. Kanemitsu, G. Uchida, D. Ichida, H. Seo, K. Kamataki, **N. Itagaki**, K. Koga, M. Shiratani, ***Proc. 8th Int. Conf. Reactive Plasmas*** (2014) 6P-AM-S08-P35.
34. "Effects of amplitude modulation on deposition of hydrogenated amorphous silicon films using multi-Hollow discharge plasma CVD method", Y. Torigoe, Y. Hashimoto, S. Toko, Y. Kim, D. Yamashita, H. Seo, **N. Itagaki**, K. Kamataki, K. Koga, M. Shiratani, ***Proc. 8th Int. Conf. Reactive Plasmas*** (2014) 6P-AM-S08-P36.
35. "Substrate temperature dependence of hydrogen content of a-Si:H film deposited with a cluster-eliminating filter", Y. Hashimoto, S. Toko, H. Seo, K. Kamataki, **N. Itagaki**, K. Koga, M. Shiratani, ***Proc. 8th Int. Conf. Reactive Plasmas*** (2014) 6P-AM-S08-P37.
36. "Sputter Deposition of Ga-doped Zinc Oxide (GZO) Films with Buffer Layers Fabricated via Nitrogen Mediated Crystallization", T. Nakanishi, K. Oshikawa, I. Suhariadi, D. Yamashita, H. Seo, K. Koga, M. Shiratani, and **N. Itagaki**, ***Proc. 8th Int. Conf. Reactive Plasmas*** (2014) 5P-AM-S05-P19.

iii) Invited talks

1. "Sputtering Growth of ZnO-based Semiconductors with Band Gap Tunability over the Entire Visible Spectrum", N. Itagaki, **Pacific Rim Symposium on Surfaces, Coatings and Interfaces**, Hawaii, USA, 16 December 2014.
2. "Sputtering Growth of High-Quality ZnO-based Semiconductors for Optoelectronic Applications", N. Itagaki, **American Vacuum Society 61st International Symposium & Exhibition**, Baltimore, USA, 13 November, 2014.
3. "Fabrication of Pseudo-binary ZnO-InN Alloys with Tunable Bandgap by Low-Temperature Magnetron Sputtering", N. Itagaki, **15th IUMRS-International Conference in Asia**, Fukuoka, Japan 29 August 2014.

4. “Sputter-deposition of pseudobinary ZnO-InN alloys with tunable bandgap for photovoltaic application”, N. Itagaki, **International Conference on Microelectronics and Plasma Technology,** Gunsan, Korea, 11 July, 2014.
5. “Novel oxynitride semiconductors for photovoltaic applications (太陽電池のための新規酸窒化物材料の探索) (presented in Japanese)”, N. Itagaki, **36th Seminar of Photovoltaic Power Generation Project (太陽光発電プロジェクト講演会)**, Miyazaki, Japan, 21 May 2014.
6. “Sputtering growth of ZnO-based semiconductors using ZnON buffer layers for optoelectronic applications”, N. Itagaki, **The International Symposium on Plasma-Nano Materials and Processes**, Seoul, Korea, 3 April 2014.
7. “N. Itagaki, K. Matsushima, I. Suhariadi, D. Yamashita, H. Seo, G. Uchida, K. Koga, M. Shiratani, Sputtering growth of single-crystalline ZnO-based semiconductors on lattice mismatched substrates, **International Society for Optics and Photonics, Photonics West 2014**, The Moscone Center, San Francisco, USA, 3 February 2014.